Annals of Nuclear Energy 38 (2011) 1645–1657

Contents lists available at ScienceDirect

Annals of Nuclear Energy

journal homepage: www.elsevier.com/locate/anucene

Void reactivity decomposition for the Sodium-cooled Fast Reactor in equilibrium fuel cycle

Kaichao Sun [a,b,*], Jiri Krepel [a], Konstantin Mikityuk [a], Sandro Pelloni [a], Rakesh Chawla [a,b]

[a] Paul Scherrer Institut (PSI), 5232 Villigen PSI, Switzerland
[b] Ecole Polytechnique Fédérale de Lausanne (EPFL), 1015 Lausanne, Switzerland

ARTICLE INFO

Article history:
Received 18 November 2010
Received in revised form 21 February 2011
Accepted 23 February 2011
Available online 29 March 2011

Keywords:
SFR
Equilibrium fuel cycle
Void reactivity
Decomposition
Neutron balance

ABSTRACT

The Sodium-cooled Fast Reactor (SFR) is one of the most promising Generation IV systems with many advantages, but has one dominating neutronic drawback – a positive sodium void reactivity. The aim of this study is to develop and apply a methodology, which should help better understand the causes and consequences of the sodium void effect. It focuses not only on the beginning-of-life (BOL) state of the core, but also on the beginning of open and closed equilibrium (BOC and BEC, respectively) fuel cycle conditions. The deeper understanding of the principal phenomena involved may subsequently lead to appropriate optimization studies.

Various voiding scenarios, corresponding to different spatial zones, e.g. node or assembly, have been analyzed, and the most conservative case – the voiding of both inner and outer fuel zones – has been selected as the reference scenario. On the basis of the neutron balance method, the corresponding SFR void reactivity has been decomposed reaction-, isotope-, and energy-group-wise. Complementary results, based on generalized perturbation theory and sensitivity analysis, are also presented. The numerical analysis for both neutron balance and perturbation theory methods has been carried out using appropriate modules of the ERANOS code system.

A strong correlation between the flux worth, i.e. the product of flux and adjoint flux, and the void reactivity importance distributions has been found for the node- and assembly-wise voiding scenarios. The neutron balance based decomposition has shown that the void effect is caused mainly by the influence of the sodium removal on the neutron spectrum, and this has been confirmed by the perturbation method. The neutron balance based decomposition has also shown that the prime consequence of the sodium voiding is the reduction of the absorption rate (especially of ^{238}U capture), which provides the strongest positive component of the void reactivity. The changes in neutron production and leakage provide smaller and negative contributions. Sensitivity analysis results for individual isotopic reactions have been found to be, in a relative sense, consistent with the neutron balance based isotope-wise decomposition. Finally, the neutron balance method has been applied to analyze the void reactivity differences between the three different SFR fuel cycle states considered, viz. BOL, BOC and BEC.

1. Introduction

The Sodium-cooled Fast Reactor (SFR) is one of the most promising candidates to meet the declared goals of the Generation IV International Forum (OECD, 2008) since, as a fast spectrum system, it enables full closure of the fuel cycle, and hence aims at an optimal management of fuel resources and the minimization of long-live radioactive wastes. In comparison to other Generation IV systems, there is considerable design experience related to the SFR, and also more than 300 reactor-years of practical operation (IAEA, 2006). Although the SFR has many advantages, it has a dominating neutronic drawback, viz. a positive reactivity effect when the sodium coolant is removed from the core, i.e. positive sodium void reactivity. The present paper reports on a decomposition study for the SFR void effect, the basic aim being to arrive at a clearer understanding of the principal contributing phenomena.

Reactivity decomposition is commonly applied in reactor analysis, and the related methodologies are well developed. They either use the neutron balance method (Chawla et al., 2008; Hong et al., 2007) or perturbation theory (Fukaya et al., 2009; Buiron et al., 2007), applications having been reported for both thermal (Chawla et al., 2008; Fukaya et al., 2009) and fast (Hong et al., 2007; Buiron et al., 2007) reactors. The perturbation theory method is widely used to assess the impact of different contributing factors to a given reactivity change and to quantify the corresponding

* Corresponding author at: Paul Scherrer Institut (PSI), 5232 Villigen PSI, Switzerland. Tel.: +41 (0) 563104554; fax: +41 (0) 563102327.
E-mail address: kaichao.sun@psi.ch (K. Sun).

0306-4549/$ - see front matter © 2011 Elsevier Ltd. All rights reserved.
doi:10.1016/j.anucene.2011.02.018

sensitivity coefficients. It requires direct and adjoint flux calculations. The neutron balance method is based on two direct flux calculations, viz. for the nominal and the perturbed cases, with all the relevant parameters being changed simultaneously in the perturbed core. Accordingly, it assumes that the individual components of the reactivity change are independent.

The neutron balance method can be used for detailed reactivity decompositions in terms of different reactions, nuclides or energy groups. However, the nominal and perturbed fluxes should be correctly normalized to ensure consistency in the comparison. The normalization is often made to the production rate (Chawla et al., 2008; Hong et al., 2007). This corresponds, in practical terms, to the same power level in the nominal and perturbed cores. An alternative approach, as adopted currently, is to normalize the neutron balance to the integral flux.

The reference SFR core design used in this study is based on the present "working horse" core of the integrated Collaborative Project on the European Sodium Fast Reactor (CP ESFR). This 3600 MWth SFR concept is being proposed by the French CEA (Blanchet et al., 2009). The active core has a pancake shape, with 4.7 m diameter and 1.0 m height. Above the active core, there is a fission gas plenum (11 cm) and then an upper steel reflector (70 cm). Below the active core, there is firstly a lower reflector (30 cm), and this is followed by a second fission gas plenum (91 cm). The fuel assemblies, consisting of pins with mixed U–Pu oxide pellets and steel cladding, are loaded into the inner and outer core zones with different Pu contents (14% and 16%, respectively). The sodium inlet and outlet temperatures are 395 °C and 545 °C, respectively.

The long-term operation of the SFR core in a closed fuel cycle will lead to an equilibrium state, where both reactivity and fuel mass flow stabilize. This assumes constant periodic fuel treatment. Similar equilibrium can be obtained also for the open (once-through) cycle operation. The present void reactivity study focuses not only on the beginning-of-life (BOL) condition of the SFR core, but also on the beginning of open and closed equilibrium (BOC and BEC, respectively) fuel cycle conditions. The EQL3D procedure (Krepel et al., 2009a) developed at PSI, and based on the ERANOS code (Ruggieri et al., 2006), has been applied to obtain these two equilibrium states. Several investigations of the sodium void effect have been reported earlier for BOL or, at most, BOC conditions, e.g. (Sciora et al., 2009; Khomyakov et al., 2009; Tommasi et al., 2010). Emphasis has accordingly been placed here on analysis of the BEC state.

The following section briefly describes the analysis methods which have been applied. Section 3 gives general results for the SFR core, while Section 4 presents the various results obtained for the void reactivity decomposition for the different fuel cycle states, in terms of reaction-, isotope- and group-wise components. Conclusions are drawn in Section 5.

2. Methods

2.1. Equilibrium fuel cycle

The open and closed cycle equilibrium conditions for the SFR core have been obtained by the EQL3D procedure (Krepel et al., 2009a). This procedure was developed in the FAST group of the Laboratory for Reactor Physics and Systems Behavior (LRS) at PSI. It is based on the ERANOS modular code (Ruggieri et al., 2006) and can be used to yield the description of two basic situations, viz. (i) the equilibrium of an open fuel cycle (result of periodic fresh fuel introduction without any recycling), and (ii) the equilibrium of a closed fuel cycle (the asymptotic state of a reactor with a fixed fuel management scheme involving recycling of its own fuel). In both cases, the explicit cycle-by-cycle reactor operation under specified periodic fuel management is simulated until the equilibrium state is reached. The fundamental assumption of the methodology is to keep the actinides mass in the manufactured fuel constant and to impose constant reactor power.

The hexagonal-z 3D geometry capability of EQL3D has been employed for the SFR core, the neutron flux being calculated using the ERANOS transport theory module VARIANT, with a simplified harmonics option and 33 energy groups. The designed specific fuel cycle length of 2050 Effective Full Power Days (EFPD) and its division into 5 batches (each of 410 EFPD) are accounted for in the simulation. It is assumed that the reshuffling and refueling period takes 30 days and that the cooling time before reprocessing is of one cycle duration ($5 \times (410 + 30) = 2200$ days). During the reprocessing, fission products (FP) from the discharged fuel, around 10% of the loaded mass, are replaced by natural uranium feed. The remaining U, Pu and minor actinides (MA) are recycled.

In most of the presented simulations, the control rods are located in the upper parking position. For the complementary studies with the perturbation theory method and sensitivity analysis, the control rods were inserted 20 cm into the active core in order to make it critical. The original core design (see Fig. 1a) with 453 fuel assemblies (225 inner/228 outer) was modified to enable the subdivision into five batches (see Fig. 1b). The modified core has three assemblies less in the outer fuel zone. The equilibrium closed fuel cycle was calculated for the design of a specific five-batch cycle. The assemblies were divided into 10 groups, as shown in Fig. 1c, viz. five for the inner zone and five for the outer zone ($5 * 45/5 * 45$). This reloading pattern was adopted from (Krepel et al., 2009b). The schematic vertical cross-section of the selected SFR core is illustrated in Fig. 4.

2.2. Voiding scenarios and spatial distribution of void reactivity importance

There are several possible scenarios for considering the coolant voiding in the SFR core, i.e. the specific core volumes assumed to have been voided in a given situation. Local voiding scenarios, either assembly- or node-wise, can help to understand the spatial distribution of the void reactivity importance, as also to investigate the possible additivity of the effects of individual voided volumes and/or their correlation with flux worth, i.e. with the product of flux and adjoint flux. Via the step-by-step assembly- or node-wise local voiding, radial and axial void reactivity importance maps have been created currently. The manner in which assembly- and node-wise voiding has been considered is illustrated in Fig. 4.

The voiding of the entire active core (both inner and outer fuel zones) was found to be effectively the most conservative case, i.e. that with the highest void reactivity. Accordingly, it has currently been selected as the reference voiding scenario for the detailed void reactivity decomposition studies carried out.

2.3. Reactivity decomposition methods

As mentioned earlier, the neutron balance method and the perturbation theory method represent the two principal approaches one may adopt for reactivity decomposition. Both have been applied in the present study.

From the basic definitions of the two methods, one sees that (i) the reactivity decomposition obtained by perturbation theory corresponds to the effects of individual reaction cross-sections and thus mainly provides an understanding for the causes of the void effect, while (ii) the neutron balance method derives the reactivity components in terms of the changes in neutron productions and losses, and thus mainly provides an understanding of the consequences. The information obtained is thus complementary.

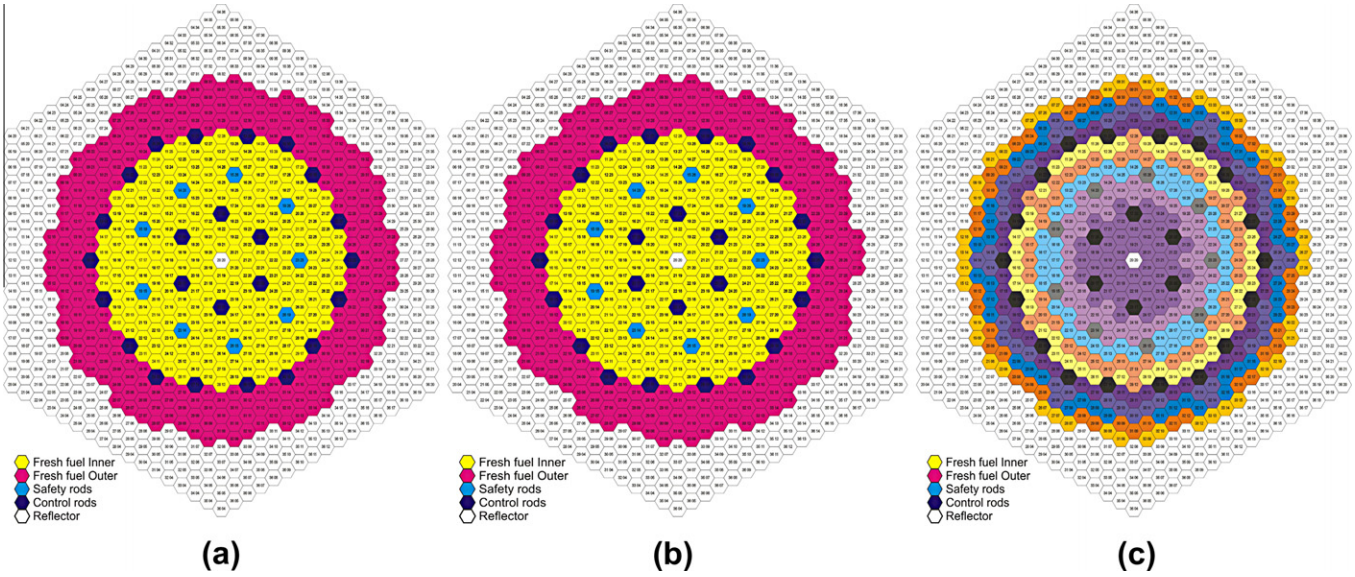

Fig. 1. Horizontal cross-sections of (a) original core design with 453 assemblies, (b) modified core design with 450 assemblies and (c) modified core with five-batch reloading pattern.

Sensitivity analysis, based on the perturbation theory method, has also been carried out currently, the results serving to underline the isotopes which are the most important for the void effect. Moreover, it has been found that the sensitivity coefficients obtained in this context for the major neutron absorbing isotopes are, in relative terms, quite consistent with the isotope-wise results of the neutron balance decomposition.

It should be noted that the numerical analysis for both neutron balance and perturbation methods has been carried out using appropriate modules of the ERANOS code system. In all cases, the flux calculations were done for hexagonal-z 3D geometry in 33 energy groups. The perturbation theory method was applied with direct and adjoint flux solutions based on diffusion theory, the standard 3D approach within ERANOS (Ruggieri et al., 2006), whereas the neutron balance method employed a transport-theory flux solution. For the sake of simplicity of the mathematical notation, a diffusion theory description is used below for both methods. Thus, the diffusion equation for $G = 33$ energy groups may be written as:

$$-\nabla D(g,r)\nabla\Phi(g,r)+\Sigma_c(g,r)\Phi(g,r)+\Sigma_f(g,r)\Phi(g,r)+\Sigma_s(g,r)\Phi(g,r)-\sum_{g'=1}^{G}(\Sigma_{g'\to g}(r)\Phi(g',r))=\frac{1}{k_{eff}}\chi(g)\sum_{g'=1}^{G}(\upsilon_{g'}\Sigma_f(g',r)\Phi(g',r)), \quad (1)$$

where the neutron flux Φ, diffusion coefficient D and macroscopic cross-sections for neutron capture Σ_c, fission Σ_f, scattering Σ_s and down scattering $\Sigma_{g'\to g}$ are all functions of the energy group g (or g') and position r. The steady-state fission spectrum $\chi(g)$ being used in the VARIANT calculations is function of only the energy group.

2.3.1. Neutron balance method

The neutron balance method for reactivity decomposition is based on the integral neutron reaction rates in the reactor core. Eq. (1) is, in this case, summed over the energy groups and integrated over space. For a consistent definition of the leakage term, the active core (AC), consisting of the inner and outer fuel zones, has been considered as the reference volume. Accordingly, the neutron balance equation can be written as:

$$-\int_{AC}\sum_{g=1}^{G}(\nabla D(g,r)\nabla\Phi(g,r))dV+\int_{AC}\sum_{g=1}^{G}(\Sigma_c(g,r)\Phi(g,r))dV+\int_{AC}\sum_{g=1}^{G}(\Sigma_f(g,r)\Phi(g,r))dV=\frac{1}{k_{eff}}\int_{AC}\sum_{g=1}^{G}(\upsilon_g\Sigma_f(g,r)\Phi(g,r))dV, \quad (2)$$

where the sum of two integrals from the scattering terms is zero and they are thus omitted. The first integral on the left-hand side of Eq. (2) represents the leakage from the active core (L). The second and third terms represent the capture (C) and fission (F) rates, respectively. (The absorption rate A is the sum of C and F). The integral on the right-hand side of the equation represents the production rate P. All these reaction rates have units of s^{-1} and relate to the active core. It should be noted that the net leakage from the active core is equal to the absorption rate outside. Using the space-energy integral of the flux (with units of cm s^{-1}) over the active core:

$$\Phi_{AC}=\int_{AC}\sum_{g=1}^{G}\Phi(g,r)dV, \quad (3)$$

the one-group core-average cross-section can be expressed as:

$$\overline{\Sigma}_x=\frac{R_x}{\Phi_{AC}}. \quad (4)$$

R (as also the corresponding subscript x) represents the selected reaction rate (L, C, F or P). Clearly, the one-group core-average cross-section for the leakage rate is to be understood in a sense analogous to the other reactions.

The neutron balance equation (Eq. (2)) can be simplified using the defined notation for the reaction rates. Replacing simultaneously k_{eff} by the reactivity ρ, one obtains:

$$\rho(L,C,F,P)=1-\frac{L+C+F}{P}. \quad (5)$$

The four reaction rates depend on the neutron flux (see Eq. (2)). The flux can be broadly characterized by the following three parameters: amplitude, the energy spectrum and spatial distribution. The amplitude is a constant, which effectively cancels out in Eq. (5). Therefore, the four reaction rates may be considered as

depending simply on the average spectrum and spatial distribution. However, each of the four can influence the neutron flux parameters, and hence also the other three. Thus, strictly speaking, the four reaction rates are somewhat interdependent.

In the present study dedicated to the void effect, the removal of sodium from the active core changes the average spectrum and spatial distribution of flux and we found that the effects of these changes are significantly stronger than the mutual influence of the variables. In other words, mutual dependencies, e.g. $\partial C/\partial L$, may be neglected in considering the corresponding reactivity change. Assuming, accordingly, the independence of the four variables in Eq. (5), the increment $\Delta\rho$ can be expressed as:

$$\begin{aligned}\Delta\rho &\equiv \rho(L_N+\Delta L, C_N+\Delta C, F_N+\Delta F, P_N+\Delta P)-\rho(L_N,C_N,F_N,P_N)\\ &= \left(\frac{\partial\rho}{\partial L}\right)_N\Delta L+\left(\frac{\partial\rho}{\partial C}\right)_N\Delta C+\left(\frac{\partial\rho}{\partial F}\right)_N\Delta F+\left(\frac{\partial\rho}{\partial P}\right)_N\Delta P\\ &\quad+\varepsilon_L\Delta L+\varepsilon_C\Delta C+\varepsilon_F\Delta F+\varepsilon_P\Delta P,\end{aligned} \tag{6}$$

where ε_x is the error term for each reaction rate change ΔX and N is a label indicating the nominal state. The error term tends to zero as ΔX tends to zero. Thus, if the changes are small $\varepsilon_x\Delta X$ can be neglected. It can be neglected also for bigger changes, but only if ρ is a linear function of the reaction rates. This is later seen to indeed be a good approximation, the reaction rate changes caused by the void effect being relatively small and the reactivity acting as an almost linear function of these. Thus, the error terms can be neglected, and the final expression for the void reactivity decomposition can be obtained by substituting Eq. (5) into Eq. (6), while expressing the derivatives in an appropriate manner:

$$\begin{aligned}\Delta\rho_V &= -\frac{1}{P_N}\Delta L-\frac{1}{P_N}\Delta C-\frac{1}{P_N}\Delta F+\frac{L_N+C_N+F_N}{P_N^2}\Delta P\\ &= -\frac{L_V-L_N}{P_N}-\frac{C_V-C_N}{P_N}-\frac{F_V-F_N}{P_N}+\frac{P_V-P_N}{P_N k_{eff,N}}\\ &= \Delta\rho_{V,L}+\Delta\rho_{V,C}+\Delta\rho_{V,F}+\Delta\rho_{V,P},\end{aligned} \tag{7}$$

where V is a label indicating the voided state.

The reaction rates used for the void reactivity decomposition have been obtained using the ERANOS neutron balance module. As already mentioned, the nominal and voided state reaction rates need to be correctly normalized to ensure consistency in the decomposition. Often the normalization used is that to the neutron production rate. This, however, effectively corresponds to the same power level in the nominal and voided states, and in this case, the production component automatically gets set to zero. An alternative approach is to normalize both cases to the integral flux. The two different normalizations can be expressed in terms of the integral flux (Eq. (3)) and the one-group core-average cross-section (Eq. (4)) as follows:

$$\begin{aligned}&\text{normalization to the production rate}: \upsilon_N\overline{\Sigma}_{f,N}\Phi_{AC,N}=\upsilon_V\overline{\Sigma}_{f,V}\Phi_{AC,V}\\ &\text{normalization to the integral flux}: \Phi_{AC,N}=\Phi_{AC,V}.\end{aligned} \tag{8}$$

Both these approaches have been tried currently. However, the constant integral flux normalization has been found preferable, because it explicitly also shows the impact of the fission rate variation. Furthermore, it directly underlines, as seen later, the changes in effective one-group cross-sections, which are parameters independent of the normalization approach.

It should be mentioned that Eq. (7) for $\Delta\rho_V$ can also be derived directly from Eq. (5) for the voided and nominal states. The only difference in the resulting expression is the appearance of $k_{eff,V}$ instead of $k_{eff,N}$, and, as expected, the two expressions are very similar for small perturbations. However, the derivation described above better demonstrates the necessary conditions for the validity of the decomposition. Thus, for example, since Eq. (7) may in general be applied to any given reactivity change, it is always important to assess the assumption of independency of the variables beforehand, this being one of the necessary conditions.

The decomposition given by Eq. (7) can be called reaction-wise. However, the reaction rates can be further divided into contributions of individual isotopes or energy groups. For the capture rate term, for example, the corresponding void reactivity components can be expressed by the following two equations:

$$\begin{aligned}\Delta\rho_{V,C} &= -\frac{\Delta C}{P_N}=-\frac{\Delta C_{U238}}{P_N}-\frac{\Delta C_{Pu239}}{P_N}-\frac{\Delta C_{Pu241}}{P_N}-\cdots-\frac{\Delta C_{Na23}}{P_N}\\ \Delta\rho_{V,C} &= -\frac{\Delta C}{P_N}=-\frac{\Delta C_{g1}}{P_N}-\frac{\Delta C_{g2}}{P_N}-\frac{\Delta C_{g3}}{P_N}-\cdots-\frac{\Delta C_{gG}}{P_N}\end{aligned} \tag{9}$$

It may be noted that the ERANOS output options would in principle also allow combined isotope- and group-wise decomposition. This, however, is not being presented here.

2.3.2. Perturbation theory and sensitivity analysis

Perturbation theory is also widely used to compute partial components of the reactivity and to quantify the sensitivity of a multivariable function to the individual variables. It requires direct and adjoint flux calculations. To express the reactivity change introduced by a perturbation, Eq. (1) will be firstly simplified by introducing two operators:

$$A(g,r)\Phi(g,r)=\frac{1}{k_{eff}}F(g,r)\Phi(g,r), \tag{10}$$

where operator A includes all terms on the left-hand side of Eq. (1) and F is the neutron production operator. Using this nomenclature and omitting the labeling for energy and space dependencies, the reactivity change can be expressed, based on exact perturbation theory, as follows:

$$\begin{aligned}\delta\rho &= \frac{\int_V\sum_{g=1}^G\left(\left(k_p^{-1}\delta F\Phi_p+\delta A\Phi_p\right)\Phi^+\right)dV}{\int_V\sum_{g=1}^G(F\Phi_p\Phi^+)dV}\\ &= \delta\rho_L+\delta\rho_P+\delta\rho_C+\delta\rho_F+\delta\rho_S,\end{aligned} \tag{11}$$

where Φ^+ is the adjoint nominal flux and Φ_p is the direct perturbed flux. The partial components for leakage $\delta\rho_L$, production $\delta\rho_P$, capture $\delta\rho_C$, fission $\delta\rho_F$ and scattering $\delta\rho_S$ can be obtained by inserting the expression for A from Eq. (1) and splitting the integrals into the partial terms. The last four mentioned components relate to perturbation of the corresponding cross-sections in Eq. (1).

The application of perturbation theory for assessing the sensitivity of the void reactivity to individual variables has been done with respect to isotope-specific reactions. Thus, the group dependent sensitivity coefficients of the void reactivity $S_{rng}(\Delta\rho_V)$ have been evaluated for a selected reaction type r for isotope n in energy group g, according to:

$$S_{rng}(\Delta\rho_V)=\frac{\delta(\Delta\rho_V)}{\Delta\rho_V}\Big/\frac{\delta\sigma_{rng}}{\sigma_{rng}}, \tag{12}$$

where $\delta(\Delta\rho_V)$ represents the impact of a variation of the selected cross-section σ_{rng} on the void reactivity $\Delta\rho_V$. As discussed later, the sensitivity coefficients obtained in this context for the major neutron absorbing isotopes have been found to be qualitatively consistent with the isotope-wise results of the neutron balance decomposition.

3. General results for the SFR core

3.1. Equilibrium fuel cycle

As mentioned earlier, this study focuses not only on the BOL state of the SFR core, but also on its BOC and BEC states, the equilibrium conditions for the latter having been obtained by the EQL3D procedure (Krepel et al., 2009b). Although, alone the equilibrium cycle

simulation and its results are interesting and could be discussed more fully, this is not currently the main objective. Accordingly, only the evolutions of nominal and void reactivities during the first and equilibrium, open and closed, fuel cycles are presented here.

Fig. 2a compares the reactivity variation during the cycle for the nominal core in each of the considered cases. It is seen that the BOL and BOC reactivities are quite comparable, but that the BEC reactivity is higher by more than 4000 pcm (1 pcm = 10^{-5}). This increased nominal reactivity is caused by the higher Pu content in the equilibrium closed fuel cycle, which is related to the core's breeding capability. The evolution of the sodium void reactivity, i.e. of the difference between the reactivities of the nominal and voided cores is shown in Fig. 2b. It is seen that the BOL void reactivity is lower than the BOC and BEC values, which are close to each other. Furthermore, the difference in void reactivity between the fuel cycles is greater at the beginning of cycle than at the end, making the comparison between BOC and BEC more meaningful than between EOC and EEC.

Table 1 gives the core reactivity values for nominal and voided states (ρ_N and ρ_V, respectively), as also their difference – the void reactivity ($\Delta\rho_V$) – for different fuel cycle states together with the corresponding global fuel composition in terms of U, Pu, MA and FP masses. It is seen, as mentioned above, that the Pu mass increases in the BEC state, which causes the reactivity increase. Furthermore, the void reactivity increases from 1578 pcm at BOL to 1978 pcm at BOC, and then further to 2050 pcm at BEC. These differences will be analyzed and explained later.

The void reactivity analysis for the BEC state is a principal goal of the present study. Nevertheless, comparisons with BOL and BOC are often made for the various results obtained, from both the neutron balance and perturbation theory methods.

3.2. Spatial distribution of void reactivity importance

Various voiding scenarios, corresponding to sodium removal from different spatial zones, have been analyzed. Thus, both radial and axial void reactivity importance maps have been created by carrying out a step-by-step, assembly- and node-wise voiding of the core. The radial void reactivity importance distribution for the BEC state is presented in Fig. 3, where one third of the symmetric core is shown. Fig. 4 gives the axial map, in terms of the distribution for a central vertical cut of the core.

The two maps clearly show that high void worths occur at the center of the active core, with much lower values at the core periphery. The fact that the local void reactivity importance is strongly correlated with the neutron flux worth distribution is confirmed by Fig. 5. This compares the radial assembly-wise distributions of the flux worth ($\Phi \cdot \Phi^+$) and of the void reactivity importance, local values being expressed relative to the volume-averaged value for the active core.

Clearly, a check on the additivity of the local void worths is of considerable interest. The reference voiding scenario, viz. voiding of the complete active core (435 fuel assemblies and 2175 calculational nodes), has been considered for the purpose. The results are presented in Table 2. As can be seen, the sum of assembly-wise void reactivity values is practically identical to the reference void reactivity, i.e. voiding of the active core. The difference is only 10 pcm. Also, the sum of node-wise void reactivity worths is in relatively good agreement with the reference void reactivity. The difference of ~80 pcm is probably caused by the nonlinear behavior of the leakage effects at the core periphery and/or numerical effects related to the size of the nodes.

4. Void reactivity decomposition

As mentioned earlier, the main part of the present study is the decomposition of the sodium void reactivity using the neutron balance based method. Results obtained applying the perturbation theory method, including the consideration of sensitivity coefficients, are presented as complementary information. The reactivity decomposition has been carried out reaction-wise, isotope-wise and energy-group-wise. Furthermore, the differences between

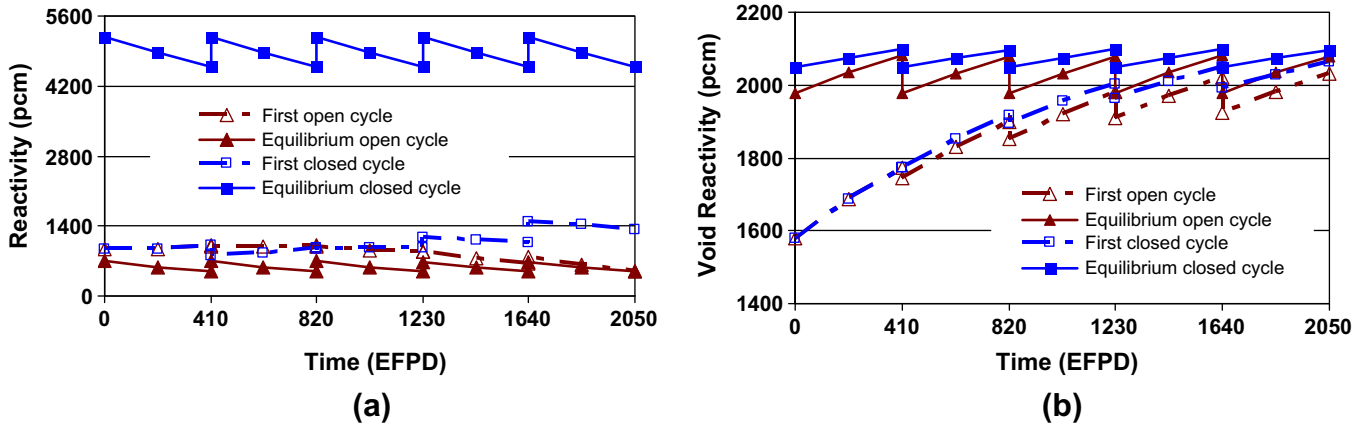

Fig. 2. Evolutions of (a) the nominal SFR core reactivity and (b) the sodium void reactivity, during the first and equilibrium, open and closed, fuel cycles.

Table 1
Nominal and voided core reactivities, their difference (void reactivity) and global fuel composition, for five selected fuel cycle states.

Fuel cycle state	ρ_N (pcm)	ρ_V (pcm)	$\Delta\rho_V$ (pcm)	U (t)	Pu (t)	MA (t)	FP (t)
Beginning of life (BOL)	933	2511	1578	61.98	11.54	0.09	0.00
Beginning of equilibrium open cycle (BOC)	693	2671	1978	58.83	11.78	0.24	2.76
End of equilibrium open cycle	490	2571	2081	57.17	11.85	0.30	4.25
Beginning of equilibrium closed cycle (BEC)	5182	7232	2050	57.73	12.42	0.63	2.74
End of equilibrium closed cycle	4585	6684	2099	56.22	12.43	0.61	4.25

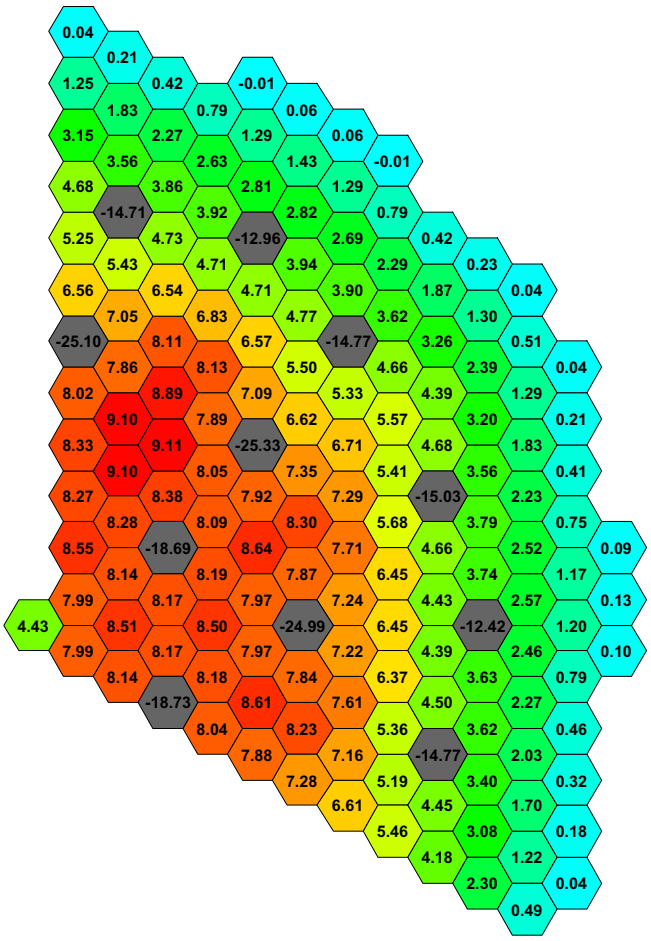

Fig. 3. Radial void reactivity importance map (units: pcm) created by step-by-step assembly-wise voiding. Results are shown for one third of the symmetric core.

BOL, BOC and BEC states have been analyzed, with BEC representing the reference case.

Table 2
Additivity check for assembly- and node-wise voiding effects, with respect to voiding of complete active core.

Voided volume	Active core	Assembly	Node
Number of volumes	1	435	2175
Av. void reactivity (pcm)	2050.2	4.69	0.91
Sum over active core (pcm)	2050.2	2040.0	1970.3

4.1. Reaction-wise decomposition

The void reactivity was decomposed reaction-wise into the $\Delta\rho_L$, $\Delta\rho_C$, $\Delta\rho_F$ and $\Delta\rho_P$ components by means of the neutron balance method using Eq. (7), and into the $\delta\rho_L$, $\delta\rho_P$, $\delta\rho_C$, $\delta\rho_F$ and $\delta\rho_S$ components by the perturbation method according to Eq. (11).

4.1.1. Neutron balance based results

The neutron balance method uses the reaction rates for nominal and voided states integrated over the active core. For better understanding of the dependency of the reactions on the sodium density, several intermediate points have also been studied. The resulting curves for the integral reaction rates and for their changes at each step are shown for the BEC state in Fig. 6a and b, respectively, Thereby, each reaction rate value has been normalized to the same integral flux Φ_{AC} (see Eq. (3)), corresponding to the nominal situation of 3600 MWth with 100% sodium density.

As Fig. 6a shows, the dependency of the reaction rates on the sodium density is not strong; the changes are relatively small and stay below 8.0% (see Table 3). Furthermore, the curves are almost linear. Thus, the main assumption for the derivation of Eq. (7) is seen to be fulfilled. The leakage rate shows the lowest variation and is increased in the voided core; the other three rates are decreased, with the capture rate showing the highest variation.

Table 3 presents the reaction rates for the nominal (100% sodium density) and voided (0% density) cores at BEC for the two different normalizations defined by Eq. (8). In addition, the table presents the effective one-group cross-sections, which are parameters independent of the normalization. It is seen that the effective capture, fission and production cross-sections are all decreased in the voided core. The decrease of the fission and production

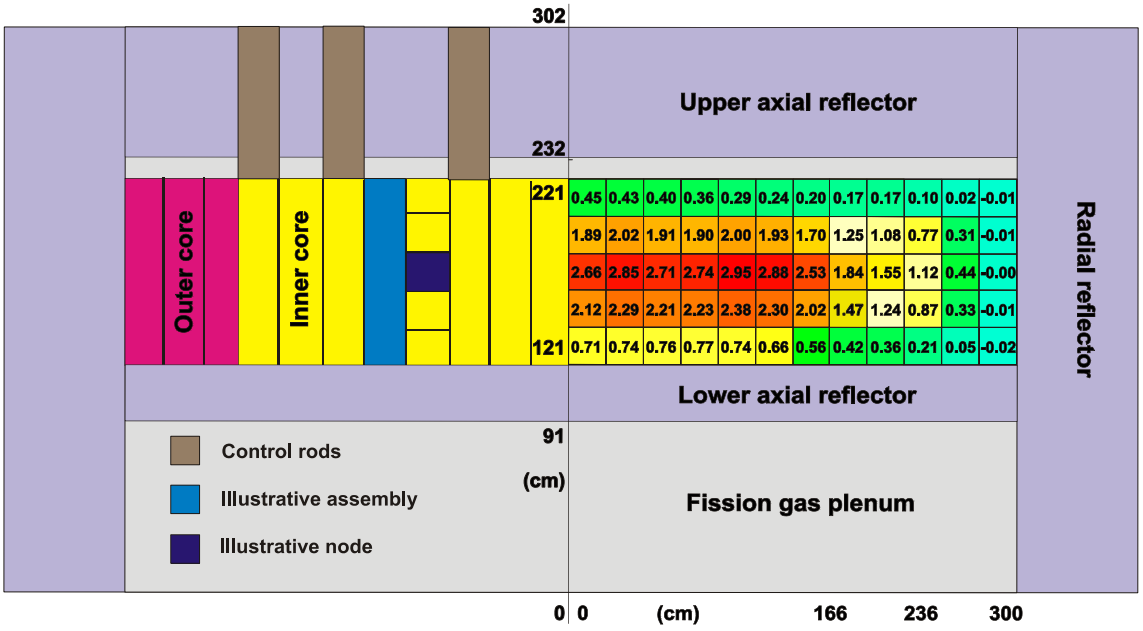

Fig. 4. Axial void reactivity importance map (units: pcm) created by step-by-step node-wise voiding. Results for a central vertical cut of the core are given on the right, the left-hand side of the figure showing a schematic of the modeling carried out.

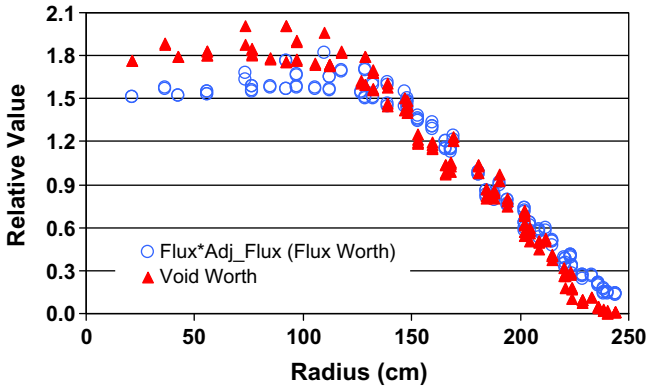

Fig. 5. Radial assembly-wise correlation of flux worth ($\Phi \cdot \Phi^{+}$) and void reactivity importance.

cross-sections is not reflected by the reaction rates, if the calculation is normalized to production. On the other hand, in the case of normalization to the integral flux, the reaction rates show the appropriate changes for all four reactions (see the relative differences indicated in Table 3). This clearly provides an important justification for choosing the latter normalization for all subsequent calculations.

For both the nominal and voided cores, there is about a 200 pcm difference for the reactivity result as obtained from the reaction rates using Eq. (5) and that derived directly from the ERANOS k_{eff} value. This is explained by the fact that the impact of (n, xn) reactions has been neglected in formulating Eq. (5). In the case of the directly derived ERANOS k_{eff} value (n, xn) events are accounted for by considering them in terms of negative captures. Nevertheless, the excellent agreement between the two different void reactivity values shown in Table 3 clearly confirms that the impact on the sodium void effect of neglecting (n, xn) reactions is quite insignificant.

Results with normalization to the integral flux, analogous to those in Table 3 for BEC, have also been obtained for the BOL and BOC states. In all three cases, transport theory was used for the neutron flux calculation and the control rods were placed in the upper parking position. The reaction-wise decomposition results for the void reactivity at BOL, BOC and BEC, as obtained using Eq. (7), are presented in Table 4.

As can be seen, for all three fuel cycle states, the capture term is the most significant positive component of the void reactivity. The production and leakage components provide smaller, negative contributions. It should be noted that a decrease in the capture, fission or leakage rate provides a positive reactivity, whereas a decrease in the production rate leads to negative reactivity; thus, the production component is always of opposite sign to the fission component, although it is $\sim\nu$-times stronger. The increases in the void reactivity for the BOC and BEC states, relative to BOL, are seen to be caused mainly by the production component. Changes in the leakage and capture components are relatively small.

4.1.2. Complementary perturbation theory based results

As mentioned earlier, the perturbation theory method for reactivity decomposition has been applied using diffusion-theory flux solutions for the core, with the control rods inserted 20 cm to assure criticality. The reaction-wise decomposition results for BOL condition, obtained using Eq. (11), are summarized in Table 5a. Shown in Table 5b are the neutron balance based results obtained

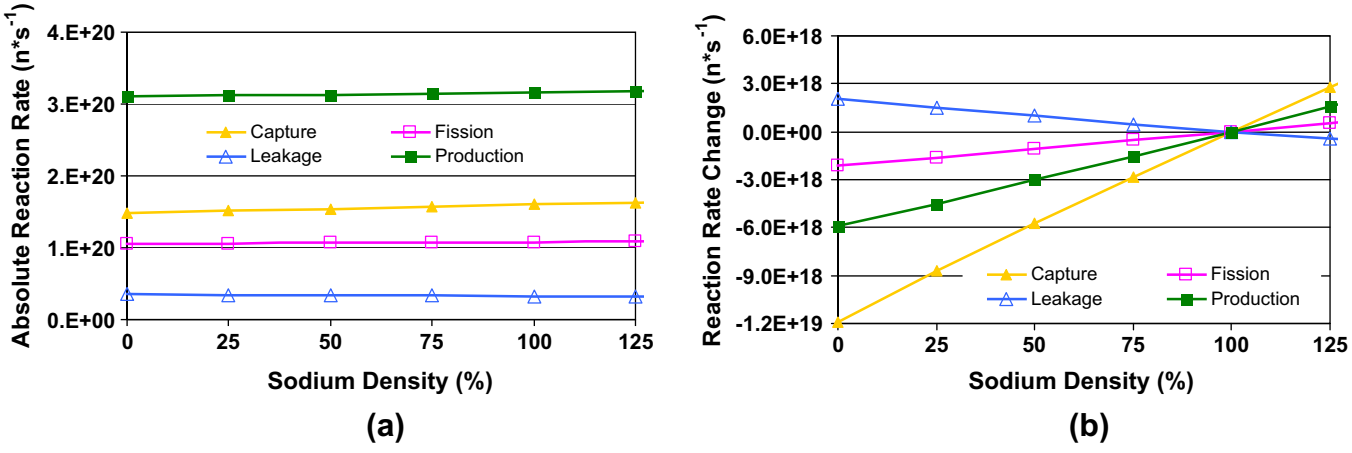

Fig. 6. Dependence of (a) integral reaction rates and (b) their absolute changes on the sodium density for the BEC state.

Table 3
Reaction rates (with different normalizations) and one-group effective cross-sections for the nominal and voided core at BEC.

BEC state	Nominal core			Voided core			Relative difference		
Variable	Rate (s^{-1})	Rate (s^{-1})	$\overline{\Sigma}_x$ (cm^{-1})	Rate (s^{-1})	Rate (s^{-1})	$\overline{\Sigma}_x$ (cm^{-1})	Δ rate (%)	Δ Rate (%)	$\Delta\overline{\Sigma}_x$ (%)
Normalization to	Φ_{AC}	Production	–	Φ_{AC}	Production	–	Φ_{AC}	Production	–
Production	3.16E+20[a]	1000	8.04E−03	3.10E+20	1000	7.89E−03	−1.9	0.0	−1.9
Leakage	3.29E+19	104.1	8.37E−04	3.50E+19	112.7	8.89E−04	5.9	8.3	5.9
Capture	1.60E+20	505.4	4.06E−03	1.48E+20	476.7	3.76E−03	−8.0	−5.7	−8.0
Fission	1.08E+20	340.5	2.74E−03	1.06E+20	340.3	2.68E−03	−2.0	−0.1	−2.0
Φ_{AC} (n cm/s)	3.94E+22	1.24E+05	–	3.94E+22	1.27E+05	–	0.0	2.4	–
ρ, Eq. (5) (pcm)	ρ_N = 4994.4			ρ_V = 7039.0			$\Delta\rho_V$ = 2044.6		
ρ, ERANOS (pcm)	ρ_N = 5181.8			ρ_V = 7232.2			$\Delta\rho_V$ = 2050.4		

[a] $E + x$ is used for 10^x in certain tables and figures, e.g. $3.16E + 20 = 3.16 \times 10^{20}$.

Table 4
Reaction-wise void reactivity decomposition by the neutron balance method and comparison of the BOL, BOC and BEC states.

Flux calculation Control rod position	Transport theory Upper parking position		
Fuel cycle state Decomp. method Normalization to	BOL Neutron balance Φ_{AC}	BOC	BEC
Leakage	−655	−610	−647
Capture	3841	3965	3759
Fission	911	788	659
Production	−2566	−2215	−1764
Component sum	1530	1928	2007

Table 5
Reaction-wise void reactivity decomposition at BOL (a) with the perturbation method and (b) with the neutron balance method.

(a)	
Decomp. method	Perturbation
Flux calculation	Diffusion theory
Control rod position	20 cm in the core
Fuel cycle state	BOL
Leakage	−789
Capture	378
Fission + Production	65
Scattering	1757
Component sum	1411
(b)	
Decomp. method	Neutron balance
Flux calculation	Diffusion theory
Control rod position	20 cm in the core
Fuel cycle state	BOL
Leakage	−751
Capture	3815
Fission	892
Production	−2534
Component sum	1422

using the same (i.e. diffusion-theory) solution for the direct flux. Before discussing the results, it should be recalled that the perturbation theory and neutron balance methods basically provide two complementary sets of reactivity components. While the former helps quantify the impact of the various cross-sections and thus provides an understanding of the causes of the reactivity change, the latter provides an understanding of the consequences.

The results in Table 5 clearly show the consistency of the two decomposition methods in the sum of the individual components. However, the partial components strongly differ.

The perturbation theory method identifies scattering as the largest positive component, which is only partly reduced by the leakage term. This implies that the reduction in scattering reactions (due to sodium removal) and the resulting spectrum hardening represent the main cause of the void effect. The neutron balance based decomposition, on the other hand, shows the capture component to be the most important positive contribution to the void reactivity. In this context, the capture rate losing is to be seen as the most important consequence of the spectrum hardening resulting from the sodium removal, even though, according to the perturbation method, the change of the capture cross-section is relatively small. Both these aspects – cause and consequence – are discussed in greater detail in the following subsection.

4.2. Isotope-wise decomposition

The void reactivity can be decomposed further isotope-wise. For the neutron balance based method, this is accomplished by applying Eq. (9), and this is currently the main focus. With the perturbation theory method, an isotope-wise consideration of the reactivity change consistent with the neutron balance method is best made via the sensitivity coefficients defined by Eq. (12).

4.2.1. Neutron balance based results

The isotope-wise decomposition by the neutron balance method is based on the individual isotopic reaction rates for capture, fission and production. These rates at BEC are shown in Fig. 7a for several key isotopes. The production rate of ^{239}Pu, which is the main fissile isotope, is seen to have the largest value. Since the reaction rates in Fig. 7a correspond to the equilibrium closed cycle state, the ^{238}U capture rate – as the "producer" reaction for ^{239}Pu – is practically equal to the ^{239}Pu destruction rate (via fission and capture), the equilibrium SFR core's behavior being nearly that of an iso-breeder with account for fuel reprocessing and refueling time.

Fig. 7b shows the changes in the isotopic reaction rates caused by the voiding of the core at BEC. The ^{238}U capture rate is seen to have the largest reduction. ^{239}Pu, as the other principal nuclide, shows significant changes in all three reaction rates.

4.2.1.1. Global isotope-wise decomposition. Isotopic reaction rate results analogous to those for BEC were also obtained for BOL and BOC. All three sets were then used for the isotope-wise void reactivity decomposition. The leakage component clearly does not warrant further decomposition in the current context, so that the global isotope-specific impact can be written as $\Delta\rho_{P,C,F} = \Delta\rho_P + \Delta\rho_C + \Delta\rho_F$. The isotope-wise decomposition for this global impact is presented in Table 6, together with the corresponding value of the component expressed per unit mass of the isotope in the given fuel cycle state.

It is seen that, for all three fuel cycle states, ^{238}U provides the largest positive reactivity component. The two other less strongly fissionable isotopes, ^{240}Pu and ^{242}Pu, increase the void reactivity as well. Conversely, the fissile isotopes ^{239}Pu and ^{241}Pu reduce the void effect. It is interesting to note that, in terms of the effect per unit mass, ^{241}Pu is found to be the most favorable isotope for reduction of the void effect reduction, while the minor actinides (MA) are the most detrimental. The difference in void reactivity between BOL, BOC and BEC results from various effects, and these are discussed separately later in the context of the more detailed decomposition presented below.

4.2.1.2. Reaction- and isotope-wise decomposition. The isotope-wise reaction rates provided by ERANOS are also divided reaction-wise. This enables one to achieve a more detailed decomposition of the void reactivity, viz. both reaction- and isotope-wise. The resulting isotope-wise decomposition of each of the three reaction rate components – $\Delta\rho_P$, $\Delta\rho_C$ and $\Delta\rho_F$ – are shown in Table 7 for all three studied fuel cycle states.

It is seen that the capture component is positive for each of the fuel isotopes, consistent with the earlier noted fact that the overall capture rate is reduced in the voided core. In this context, the ^{238}U capture term is the most important single component and, as such, represents the major contribution to the positive void reactivity.

It can also be seen that the fissile isotopes all have positive fission components, which means that each of these fission rates is reduced in the voided core. The corresponding production components are negative and ν-times stronger; furthermore, each of these production components is also stronger than the corresponding capture term. Accordingly, the net impact on the void reactivity of each of the fissile isotopes (principally, ^{239}Pu and ^{241}Pu) is negative.

On the other hand, the less strongly fissionable isotopes show negative fission, and thus positive production, components. In addition, they also have their positive capture components, so that their overall impact is positive. To this group belong ^{240}Pu and

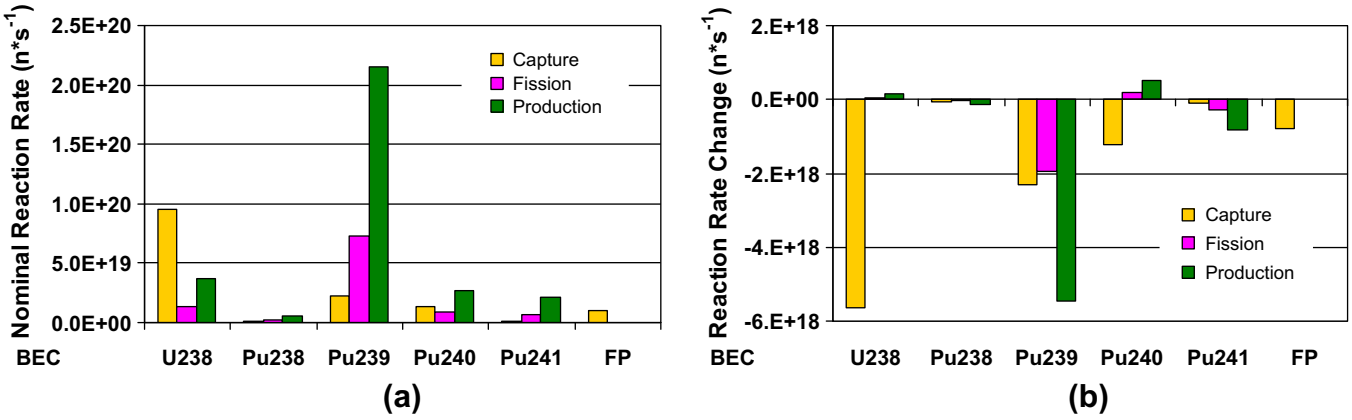

Fig. 7. Isotope-wise (a) reaction rates in the nominal core at BEC and (b) reaction rate changes caused by the core voiding.

Table 6
Global isotope-wise void reactivity decomposition for BOL, BOC and BEC states.

State	BOL			BOC			BEC		
Variable (units)	Mass, m (t)	$\Delta\rho_{P,C,F}$ (pcm)	$\Delta\rho_{P,C,F}$/m (pcm/t)	Mass, m (t)	$\Delta\rho_{P,C,F}$ (pcm)	$\Delta\rho_{P,C,F}$/m (pcm/t)	Mass, m (t)	$\Delta\rho_{P,C,F}$ (pcm)	$\Delta\rho_{P,C,F}$/m (pcm/t)
U235	0.15	−25.9	−172.7	0.11	−19.9	−180.9	0.08	−10.4	−130.0
U238	61.83	2080.8	33.7	58.70	1997.5	34.0	57.46	1814.2	31.6
Pu238	0.42	−2.9	−6.9	0.34	−6.0	−17.6	0.26	2.1	8.1
Pu239	5.51	−504.7	−91.6	6.05	−397.4	−65.7	6.97	−295.7	−42.4
Pu240	3.45	457.8	132.7	3.49	443.0	126.9	4.29	488.8	113.9
Pu241	0.96	−378.2	−394.0	0.77	−291.7	−378.8	0.46	−130.8	−284.3
Pu242	1.21	121.7	100.6	1.14	109.5	96.1	0.43	39.1	90.9
MA	0.09	26.0	288.9	0.27	62.7	232.2	0.90	136.2	151.3
FP	0.00	0.0	–	2.76	238.3	86.3	2.74	244.2	89.1
O16	9.79	−2.0	−0.2	9.79	−2.1	−0.2	9.79	−2.6	−0.3
Na23	4.03	133.5	33.1	4.03	131.3	32.6	4.03	120.8	30.0
Steel	22.98	279.5	12.2	22.98	272.0	11.8	22.98	248.0	10.8
SUM	110.4	2185.6	19.8	110.4	2537.2	23.0	110.4	2653.8	24.0

Table 7
Reaction- and isotope-wise void reactivity decomposition for BOL, BOC and BEC.

State	BOL			BOC			BEC		
Variable (units)	$\Delta\rho_P$ (pcm)	$\Delta\rho_C$ (pcm)	$\Delta\rho_F$ (pcm)	$\Delta\rho_P$ (pcm)	$\Delta\rho_C$ (pcm)	$\Delta\rho_F$ (pcm)	$\Delta\rho_P$ (pcm)	$\Delta\rho_C$ (pcm)	$\Delta\rho_F$ (pcm)
U235	−76.2	18.6	31.7	−55.9	12.9	23.1	−32.7	8.1	14.2
U238	36.5	2056.2	−12.0	24.9	1980.4	−7.9	44.3	1785.4	−15.6
Pu238	−80.4	49.0	28.4	−66.4	37.1	23.3	−35.4	24.4	13.2
Pu239	−1894.2	718.6	670.9	−1737.5	723.6	616.5	−1639.4	733.3	610.3
Pu240	109.0	385.5	−36.6	118.3	364.3	−39.6	157.2	386.4	−54.9
Pu241	−696.7	78.1	240.4	−534.4	58.9	183.9	−252.7	30.6	91.4
Pu242	34.8	98.6	−11.7	31.5	88.6	−10.5	14.0	29.9	−4.9
MA	1.2	25.2	−0.3	4.4	59.6	−1.3	−19.7	150.3	5.5
FP	–	0.0	–	–	238.3	–	–	244.2	–
O16	–	−2.0	–	–	−2.1	–	–	−2.6	–
Na23	–	133.5	–	–	131.3	–	–	120.8	–
Steel	–	279.5	–	–	272.0	–	–	248.0	–
SUM	−2566.1	3840.8	910.8	−2215.2	3964.8	787.6	−1764.3	3758.8	659.4

^{242}Pu, as also the already discussed ^{238}U with its very strong capture component. Regarding the non-fuel materials, the capture reactivity component for steel is twice higher than that for the void-effect steering isotope ^{23}Na, which has only minor impact. At BOC and BEC, there is also a significant positive capture term for the fission products (FP).

4.2.1.3. Differences between BOL, BOC and BEC. Table 7 also shows in detail the origin of the void reactivity differences between the BOL, BOC and BEC states. Before discussing the various individual effects, it is instructive to first compare the differences in the nominal reaction rates between BOC and BOL, and between BEC and BOC. From the results shown in Fig. 8a, it is seen that the BOC reaction rates differ from the BOL values mainly in terms of the higher (newly appearing) FP, lower ^{238}U capture, higher ^{239}Pu, and lower ^{241}Pu fission (along with the corresponding production differences). The reaction rate differences between the BEC and BOC states shown in Fig. 8b indicate that the ^{238}U capture rate is significantly lower at BEC. The fission rate (and related production) is higher for ^{239}Pu and ^{240}Pu, and lower for ^{241}Pu.

The above fuel-cycle specific difference in the nominal state of the SFR core are, as to be expected, somewhat different when one considers the change caused by voiding. These differences clearly influence the trend one sees for the void reactivity between BOL, BOC and BEC.

As presented in Table 1, the void reactivity increases from 1578 pcm at BOL to 1978 pcm at BOC, and then further to 2050 pcm at BEC. Thus, the differences are 400 pcm between BOC and BOL, and only 72 pcm between BEC and BOC. The corresponding differences in the leakage component of the void reactivity (see Table 4) are only 45 pcm and −37 pcm. Accordingly, the remaining three reactions (production, capture and fission) should contribute 355 pcm and 109 pcm to the former and latter differences, respectively. These values are quite consistent with the decomposition comparisons made in Table 7, between BOL, BOC and BEC: the differences in the sum of the production, capture and fission components of the void reactivity are seen to be 352 pcm between BOC and BOL, and 117 pcm between BEC and BOC.

Table 8 presents the decompositions of Table 7 in another form, viz. in terms of the differences in the reaction- and isotope-wise components between the three studied fuel cycle states. Thereby, it is seen that the net (BOC–BOL) difference of 352 pcm is mainly caused by the appearance of FP capture (238 pcm), and the smaller negative contributions from ^{239}Pu (107 pcm) and ^{241}Pu (87 pcm). The smaller negative ^{239}Pu contribution at BOC appears to be in contradiction to the fact that the ^{239}Pu mass is increased at BOC (see Table 8 and Fig. 8a). This is a consequence of the relatively strong neutron spectrum change. The fourth largest component of the (BOC–BOL) difference in void reactivity is the ^{238}U capture (−83 pcm). The mass of ^{238}U is decreased in the BOC state, which, in this case, is qualitatively consistent with its reduced positive contribution to the void reactivity.

As regards the (BEC–BOC) void reactivity difference of 117 pcm, Table 8 shows that this has several components of comparable magnitude. First of all, the ^{238}U mass is further reduced and simultaneously the spectrum is changed, with the result that the total ^{238}U impact is −183 pcm (−195 pcm from its capture). The ^{241}Pu mass is also further decreased, the resulting positive effect on the void reactivity being 161 pcm. The third most important isotope is ^{239}Pu (102 pcm). Its negative contribution to the void effect is reduced, again in apparent contradiction to its mass increase.

4.2.2. Comparison with sensitivity coefficients (perturbation theory based results)

As mentioned earlier, an isotope-wise decomposition of the void reactivity on the basis of the perturbation theory based method is best achieved by quantifying the corresponding sensitivity coefficients. For a given isotope X and reaction type Y, the group dependent sensitivity coefficient is obtained applying Eq. (12). Clearly, the energy integrated sensitivity coefficient (obtained from the sum of the group dependent values for a given reaction) cannot be directly compared with the corresponding reactivity component obtained from the neutron balance method. Accordingly, in order to achieve a qualitative comparison, the results for the two sets of parameters have first been normalized internally, the ^{238}U capture rate being selected as the reference in each case. Furthermore, one should note that – for the type of comparison being made here – the perturbation theory result for the sensitivity to a specific fission cross-section needs to be compared with the sum of the corresponding fission and production terms obtained from the neutron balance method.

Table 9 shows the two sets of normalized results (with the value for ^{238}U capture set at 100 in each), in terms of values for the individual isotopes. The important sensitivity coefficient with respect to scattering is not considered here, since there is no corresponding term to be compared with in the neutron balance context.

The two sets of numbers in Table 9 are, somewhat surprisingly, quite consistent, even though the coefficients serve to quantify the sensitivity of the void reactivity to the cross-section for a given reaction (i.e. provide a measure of "cause"), while the neutron balance based decomposition quantifies the impact of that reaction (i.e. provides a measure of "consequence"). The explanation is to be found in the nature of the sodium void effect. Due to the reduced ^{23}Na scattering, the spectrum is hardened quite significantly upon voiding of the core. This has a high impact on all reaction rates. In the energy region where the spectrum changes most strongly, the neutron flux is increased or decreased considerably, but the multi-group cross-sections for capture and fission stay practically constant. Accordingly, the importance of both sensitivity coefficients and neutron balance components is simply proportional to the value of the cross-section for the corresponding reaction. This aspect is discussed further in the next subsection, which considers the energy-wise decomposition of the void reactivity.

As regards the role of sodium itself, it is clear that the contribution of ^{23}Na capture is of little significance. The sensitivity coefficient and neutron balance based component for this reaction are seen in Table 9 to be only 9% and 6%, respectively, of the corresponding ^{238}U capture value. On the other hand, the values of the sensitivity coefficients with respect to sodium elastic and inelastic scattering have been found to be as high as about 75% and 44%, respectively, relative to the value for the important ^{238}U capture reaction. This of course corresponds to the high impact mentioned above, which the spectrum hardening due to sodium removal has on all reaction rates.

In summary, the reaction- and isotope-wise decompositions of the void reactivity – using the complementary, neutron balance

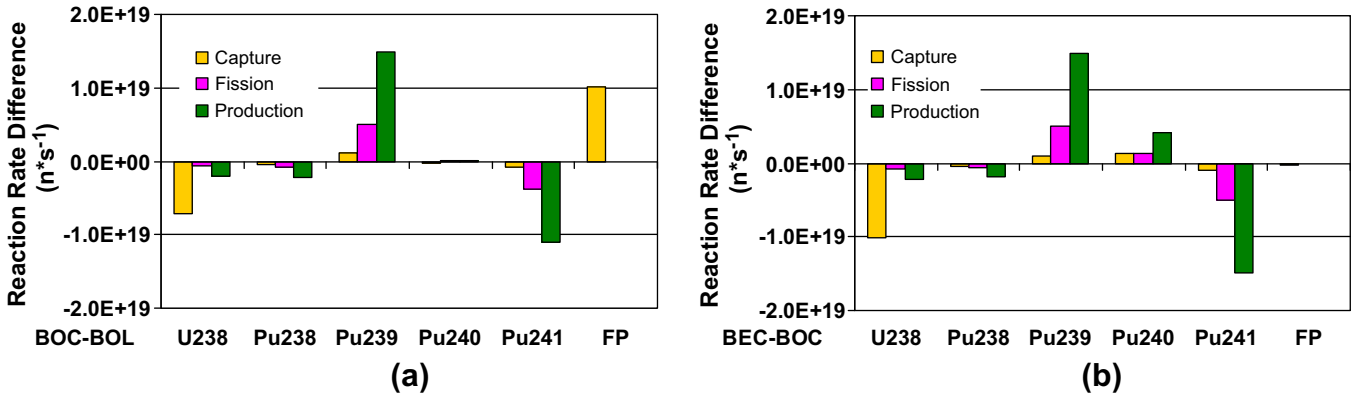

Fig. 8. Differences in nominal reaction rates between (a) BOC and BOL, and between (b) BEC and BOC.

Table 8
Differences of isotope-wise void reactivity component between the BOL and BOC and between the BOC and BEC states.

Difference	BOC–BOL					BEC–BOC				
Variable (units)	Mass (t)	$\Delta\rho_P$ (pcm)	$\Delta\rho_C$ (pcm)	$\Delta\rho_F$ (pcm)	$\Delta\rho_{P,C,F}$ (pcm)	Mass (t)	$\Delta\rho_P$ (pcm)	$\Delta\rho_C$ (pcm)	$\Delta\rho_F$ (pcm)	$\Delta\rho_{P,C,F}$ (pcm)
U235	−0.04	20.3	−5.7	−8.6	6.0	−0.03	23.2	−4.8	−8.9	9.5
U238	−3.13	−11.6	−75.8	4.1	−83.3	−1.24	19.4	−195.0	−7.7	−183.3
Pu238	−0.08	14.0	−11.9	−5.1	−3.1	−0.08	31.0	−12.7	−10.1	8.1
Pu239	0.54	156.7	5.0	−54.4	107.3	0.92	98.1	9.7	−6.2	101.7
Pu240	0.04	9.3	−21.2	−3.0	−14.8	0.80	38.9	22.1	−15.3	45.8
Pu241	−0.19	162.3	−19.2	−56.5	86.5	−0.31	281.7	−28.3	−92.5	160.9
Pu242	−0.07	−3.3	−10.0	1.2	−12.2	−0.71	−17.5	−58.7	5.6	−70.4
MA	0.18	3.2	34.4	−1.0	36.7	0.63	−24.1	90.7	6.8	63.5
FP	2.76	–	238.3	–	238.3	−0.02	–	5.9	–	5.9
O16	0.00	–	−0.1	–	−0.1	0.00	–	−0.5	–	−0.5
Na23	0.00	–	−2.2	–	−2.2	0.00	–	−10.5	–	−10.5
Steel	0.00	–	−7.5	–	−7.5	0.00	–	−24.0	–	−24.0
SUM	0.00	350.9	124.0	−123.2	351.6	0.00	450.9	−206.0	−128.2	116.6

Table 9
Normalized isotope-wise results for (a) void reactivity sensitivity coefficients to capture and fission cross-sections, (b) neutron balance based void reactivity components for capture and for the sum of fission and production; normalization, in each case, is to a value of 100 for ^{238}U capture.

Variable	$S\sigma_c$	$S\sigma_f$
(a) Void reactivity sensitivity coefficients normalized to value for ^{238}U capture		
U235	1.0	−2.9
U238	100.0	4.5
Pu238	2.8	−3.1
Pu239	40.9	−74.0
Pu240	20.4	8.4
Pu241	4.4	−32.9
Pu242	5.5	2.6
MA	1.5	0.1
O16	−1.3	–
Na23	8.7	–
Steel	2.0	–
SUM	185.8	−97.4

(b) Void reactivity decomposition components normalized to value for ^{238}U capture	$\Delta\rho_C$	$\Delta\rho_F + \Delta\rho_P$
U235	0.9	−2.2
U238	100.0	1.7
Pu238	2.4	−2.5
Pu239	34.8	−59.8
Pu240	18.7	3.7
Pu241	3.8	−22.5
Pu242	4.8	1.2
MA	1.2	0.04
O16	−0.1	–
Na23	6.4	–
Steel	13.5	–
SUM	186.4	−80.2

and perturbation theory based sensitivity coefficients – have clearly underlined the role of ^{238}U capture as the most important single reaction rate, from both the neutron balance and sensitivity analysis viewpoints. Furthermore, ^{239}Pu and ^{241}Pu fission (in conjunction with the corresponding production terms) contribute significant negative components. Finally, the important role of sodium is manifested, not directly in the neutron balance decomposition, but rather via the scattering term in the sensitivity analysis, i.e. in terms of its large influence on the neutron spectrum. This aspect is discussed in the following.

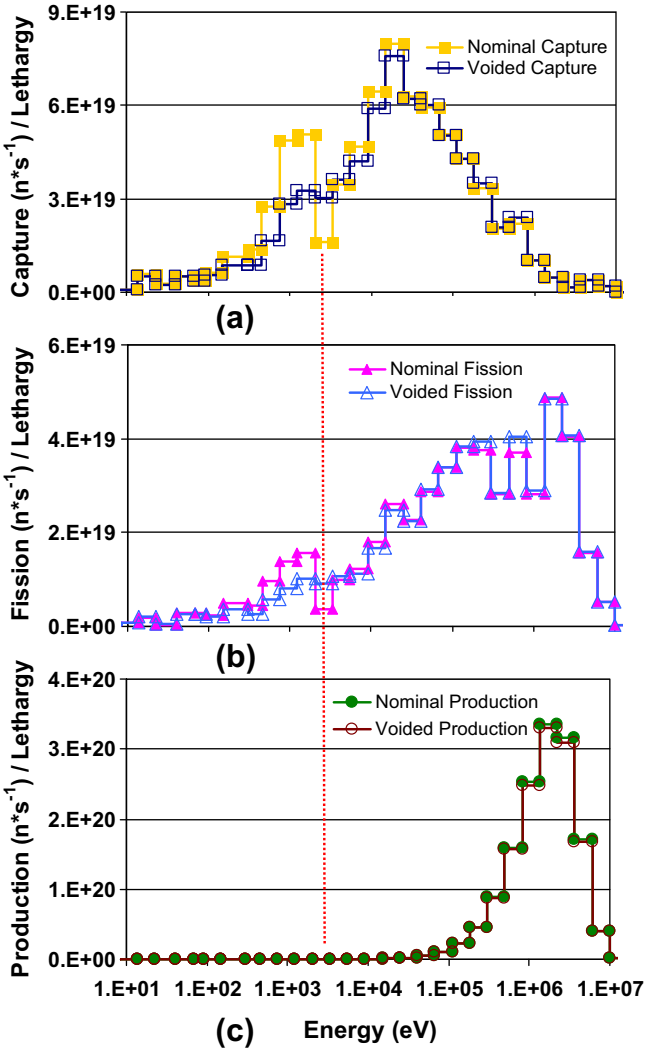

Fig. 9. Group-wise distributions for (a) capture, (b) fission and (c) production rates at BEC. The dotted red line marks the position of the ^{23}Na scattering resonance at ~3 keV.

4.3. Group-wise decomposition

To better understand the relationship between the reduced scattering (due to sodium removal) and the decreased ^{238}U capture in the voided core, the necessary group-wise reaction rates were obtained from ERANOS and the group-wise decomposition of the void reactivity was carried out applying the neutron balance method according to Eq. (9).

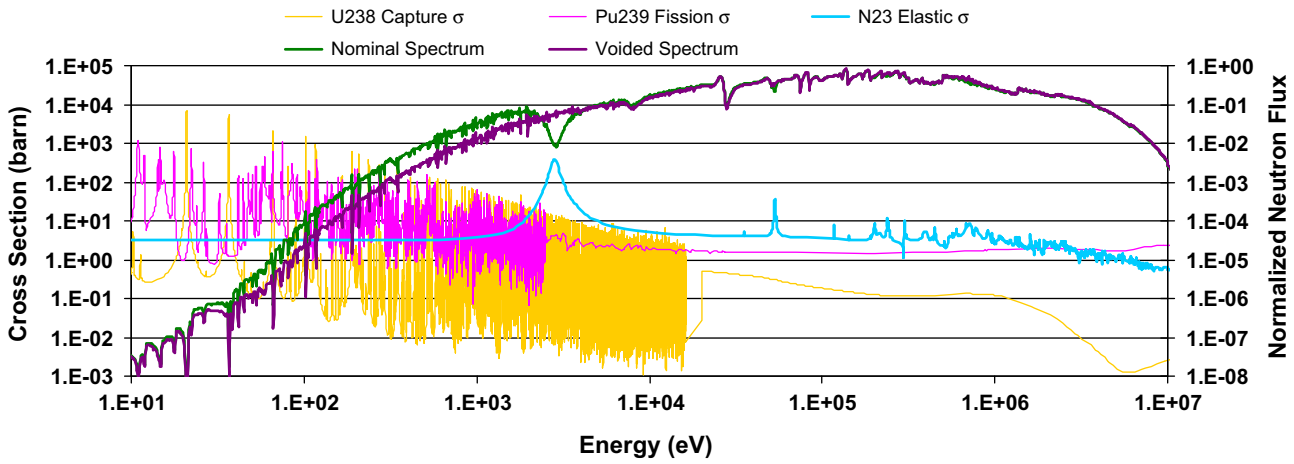

Fig. 10. Nominal and voided SFR spectra, along with ^{238}U, ^{239}Pu and ^{23}Na cross-sections.

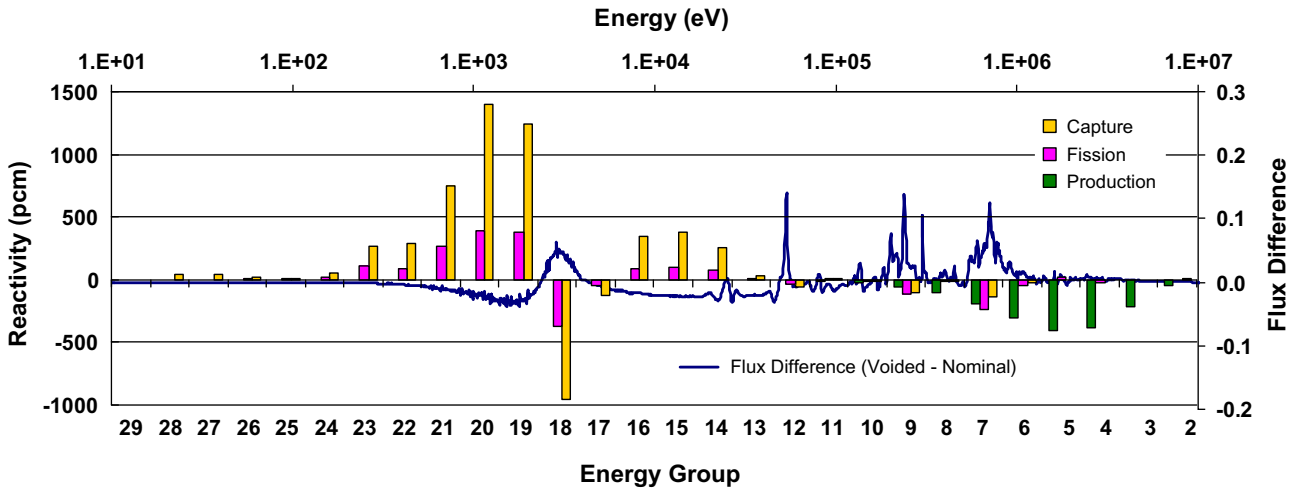

Fig. 11. Group-wise void reactivity decomposition at BEC, together with the change in neutron spectrum.

Fig. 9 first presents the energy dependence of the capture, fission and production rates in the nominal (100% sodium density) and voided (0% density) cores at BEC. It is clearly from Fig. 9a and b that the energy distributions for the capture and fission rates differ quite significantly between the two cases, the strongest variation being at and below the ^{23}Na scattering resonance at ~3 keV. As regards the production rate, illustrated in Fig. 9c, this is slightly lower in the voided core than in the nominal state, but the energy distribution – being determined by the fission spectrum – is almost identical.

In order to better understand the changes in the capture and fission rate energy distributions, the neutron spectra for the nominal and voided states were examined more closely, along with the cross-section for ^{238}U capture, ^{239}Pu fission and ^{23}Na elastic scattering. It is clearly seen from Fig. 10 that, in the nominal case, the strong sodium scattering resonance at ~3 keV suppresses the neutron flux at this energy and increases it significantly at lower energies. The spectrum in the nominal state is thus effectively shifted to an energy range with higher ^{238}U capture and ^{239}Pu fission cross-sections. In the voided core, this spectral shift disappears, and these reaction rates are reduced correspondingly. (It should be noted that the presented 1968 energy-group spectra were obtained from cell calculations for the ESFR fuel lattice, using the ERANOS module ECCO.)

The group-wise void reactivity decomposition for the BEC state is illustrated in Fig. 11. As shown, the production component, which relates to fission, provides solely negative reactivity contributions and is distributed according to the fission spectrum. The capture and fission components, on the other hand, correspond to both negative and positive reactivity values. Furthermore, these two sets of components behave consistently within each group. The most conspicuous fluctuation in sign occurs between the 18th and 19th energy group, i.e. in the region of the ^{23}Na scattering resonance where the neutron flux difference also changes sign (see the blue[1] plot in Fig. 11).

From the above discussion, it is clearly seen that the void effect is mainly driven by the spectrum shift caused by the sodium removal. Thereby, the sodium elastic scattering resonance at ~3 keV plays a key role, largely determining the influence on the capture and fission rates, and hence the corresponding void reactivity components. The reduced capture rate in the region below the sodium resonance (i.e. ~3 keV), in particular that of ^{238}U, results in being the main consequence, even though the capture cross-section in these energy groups does not change much.

[1] For interpretation of color in Figs. 1–11, the reader is referred to the web version of this article.

5. Conclusions

The sodium void effect for the SFR has been studied in this paper, emphasis being placed on the equilibrium closed fuel cycle. Voiding of the active core (both inner and outer fuel zones) was chosen as the reference voiding scenario, the void effect in the core region having been found to be spatially additive. It has also been shown that the spatial distributions of flux worth and void reactivity importance are strongly correlated.

The void reactivity for the reference voiding case has been decomposed using a methodology based on the neutron balance equation. This was done in terms of the corresponding leakage, fission, capture and production terms, as well as isotope-wise and energy-group-wise. It has been shown that the dominating component of the void reactivity is the strongly positive absorption term, whereas the negative production and leakage terms are relatively weaker. ^{238}U capture is the dominating reaction rate. ^{239}Pu, as the second most important nuclide, yields significant contributions due to changes in both production and absorption. However, these two partly compensate each other, and the overall negative effect is significantly smaller in magnitude than the ^{238}U capture effect. It is necessary to note that the impact of ^{23}Na capture is negligible. In terms of the impact per unit mass, ^{241}Pu has been found to be the most favorable isotope for reduction of the void reactivity.

The void effect is driven mainly by the strong ^{23}Na elastic scattering resonance at $\sim$3 keV, which in the nominal case suppresses the neutron flux at this energy and increases it significantly at lower energies. The spectrum is thus shifted to the energy range with higher ^{238}U capture and ^{239}Pu fission cross-sections. In the voided core, this spectral shift disappears, resulting in the reduction of both ^{238}U capture and ^{239}Pu production (in conjunction with fission), and yielding the corresponding important contributions to the reactivity change.

The decomposition results obtained applying the perturbation theory method have confirmed the key role played by ^{23}Na scattering. In addition, the isotope-wise sensitivity analysis results for capture, fission and production have been found to be quite consistent, in relative terms, with the corresponding components obtained from the isotope-wise neutron balance based decomposition.

As compared to the beginning-of-life (BOL) void reactivity value of $\sim$1578 pcm for the considered SFR core, the influences of equilibrium closed and open fuel cycles on the void reactivity correspond to increases of $\sim$468 pcm (BEC) and $\sim$352 pcm (BOC), respectively. The four most important isotope-wise contributions to these influences are those of the fission products, ^{238}U, ^{241}Pu and ^{239}Pu, the overall impact of the minor actinides not being very significant.

Finally, it should be mentioned that the decomposition methodology which has been developed and applied here is not only of help in achieving a better understanding of the SFR void reactivity, but is also proving to be a valuable tool for certain optimization studies currently in progress.

References

Blanchet, D. et al., 2009. ESFR 'Working Horses' Core Concept Definition, FP7 EURATOM ESFR Project Deliverable SP2.1.2.D1. CEA, Cadarache.

Buiron, L. et al., 2007. Innovative core design for generation IV sodium-cooled fast reactors. In: Proceedings of ICAPP 2007, Nice, France, May 13–18, Paper 7383.

Chawla, R. et al., 2008. Diagnostic analysis of pin-removal reactivity worth experiments in a SVEA-96+ test lattice. Annals of Nuclear Energy 35, 495–502.

Fukaya, Yuji et al., 2009. Study on characteristics of void reactivity coefficients for high-conversion-type core of FLWR for MA recycling. Journal of Nuclear Science and Technology 46 (8), 819–830.

Hong, Ser Gi et al., 2007. Neutronic characterization of sodium-cooled fast reactor in an MHR-SFR synergy for TRU transmutation. In: Proceedings of ICAPP 2007, Nice, France, May 13–18, Paper 7308.

IAEA, 2006. Fast Reactor Database. <http://www-frdb.iaea.org/>.

Khomyakov, Yu S. et al., 2009. Optimization of parameters of MOX fuel core of sodium cooled large size fast reactor. In: Proceedings of GLOBAL 2009, Paris, France, September 6–11, Paper 9235.

Krepel, J., Pelloni, S., Mikityuk, K., Coddington, P., 2009a. EQL3D: ERANOS based equilibrium fuel cycle procedure for fast reactors. Annals of Nuclear Energy 36 (5), 550–561.

Krepel, J., Mikityuk, K., Sun, K., Rimpault, G., 2009b. SFR equilibrium cycle analysis with the EQL3D procedure. In: Proceedings of ICAPP 2009, Tokyo, Japan, May 10–14, Paper 9226.

OECD, 2008. Nuclear Energy Agency, Generation IV International Forum Annual Report.

Ruggieri, J.M. et al., 2006. ERANOS 2.1: international code system for GEN IV fast reactor analysis. In: Proceedings of ICAPP 2006, Reno, NV USA, June 4–8, Paper 6360.

Sciora, P. et al., 2009. A break even oxide fuel core for an innovative french sodium-cooled fast reactor: neutronic studies results. In: Proceedings of GLOBAL 2009, Paris, France, September 6–11, Paper 9528.

Tommasi, J. et al., 2010. Validation of the sodium void reactivity effect prediction using JEFF-3.1 nuclear data. Annals of Nuclear Energy 37 (11), 1534–1553.